



HAL
open science

A method using near infrared hyperspectral imaging to highlight the internal quality of apple fruit slices

Weijie Lan, Benoit Jaillais, Catherine M.G.C. Renard, Alexandre Leca, Songchao Chen, Carine Le Bourvellec, Sylvie Bureau

► To cite this version:

Weijie Lan, Benoit Jaillais, Catherine M.G.C. Renard, Alexandre Leca, Songchao Chen, et al.. A method using near infrared hyperspectral imaging to highlight the internal quality of apple fruit slices. *Postharvest Biology and Technology*, 2021, 175 (1), pp.111497. 10.1016/j.postharvbio.2021.111497 . hal-03182741

HAL Id: hal-03182741

<https://hal.inrae.fr/hal-03182741v1>

Submitted on 13 Feb 2023

HAL is a multi-disciplinary open access archive for the deposit and dissemination of scientific research documents, whether they are published or not. The documents may come from teaching and research institutions in France or abroad, or from public or private research centers.

L'archive ouverte pluridisciplinaire **HAL**, est destinée au dépôt et à la diffusion de documents scientifiques de niveau recherche, publiés ou non, émanant des établissements d'enseignement et de recherche français ou étrangers, des laboratoires publics ou privés.



Distributed under a Creative Commons Attribution - NonCommercial 4.0 International License

29 **Highlights**

30 Near-infrared hyperspectral imaging assessed the apple heterogeneity.

31 Principal component analysis allowed to select the region of interest in apples.

32 Single apple presented a large heterogeneity of biochemical compositions.

33 Models mapped total sugars and dry matter contents in each apple.

34

35 **Abstract**

36 The heterogeneity of apple fruit was highlighted by near-infrared hyperspectral
37 imaging (NIR-HSI) using a data analysis in two successive steps. First, NIR-HSI
38 images were acquired on the cut surface of six transverse slices per apple, which were
39 then systematically sampled with 5 or 6 cylinders per slice. PCA carried out on the
40 NIR-HSI images allowed to select 141 representative cylinders from the total dataset
41 (1056 samples), in which the contents of dry matter (DMC), total sugars (TSC),
42 fructose, glucose, sucrose, malic acid and polyphenols were quantified by
43 spectrophotometry and chromatography. In a second step, leave-one-out PLS models
44 were developed and successfully used to describe the distribution of DMC ($R_{cv}^2 =$
45 0.83, RPD = 2.39) and TSC ($R_{cv}^2 = 0.81$, RPD = 2.20) in each apple slice. A strong
46 heterogeneity of DMC and TSC was detected inside each fruit. Such a simple and
47 rapid method reduced the needs of numerous chemical characterizations to
48 demonstrate the distribution of quality traits within and between fruit and contributed
49 to better manage the fruit quality measurements.

50 **Keywords:** *Malus domestica* Borkh.; partial least square regression; random forest
51 regression; apple variability and heterogeneity.

52

53 **Introduction**

54 An external aesthetic appearance and a sustainable internal quality of fruit are
55 both crucial for consumers (Ma et al., 2018; Zhang et al., 2018). However, genetic
56 diversity (varieties), pedoclimatic conditions and agricultural practices are known to
57 provide variability and heterogeneity of fruit, which limit the precision and prediction
58 of quality using infrared methods (Vis-NIR and NIRS) and thus hinders their
59 widespread applications for online commercial fruit sorting (Barritt et al., 1991; Xia et
60 al., 2020; Zhang et al., 2018). It appears necessary to develop some applications using
61 efficient and rapid technologies to phenotype internal heterogeneity of the fruit, in
62 order to help field growers and industrial manufacturers to improve quality of fruit
63 products.

64 Apple is one of the most consumed agricultural commodities in the global fruit
65 market (68.6 million tons at 2018) (USDA, 2018). The high heterogeneity of soluble
66 solids content (Fan et al., 2016; Mo et al., 2017; Peiris et al., 1999), starch (Menesatti
67 et al., 2009), polyphenols and vitamin C (Pissard et al., 2012) in a single apple fruit
68 has been proven to truly exist in different directions, from proximal to distal direction
69 (Fan et al., 2016; Peiris et al., 1999), in radial direction from inside to outside (Mo et
70 al., 2017) and along equatorial direction (Mo et al., 2017; Pissard et al., 2012).

71 As known, conventional chemical analyses (HPLC-DAD, GC-MS and
72 ultraviolet/ visible spectrometry etc.) are costly and time-consuming to determine the
73 heterogeneity occurring at the level of the tissues in a single fruit (Peng et al., 2019;
74 Pissard et al., 2012). To determine the chemical heterogeneity within a fruit, most

75 previous works encountered difficulties of i) long-periods and intensive labor
76 operations, ii) a large amount of targeted fruit samples and the high requirements for
77 characterization, and iii) the limited stability of fruit samples (highly hydrated, rapid
78 oxidation). In addition, the limited knowledge of apple heterogeneity becomes a
79 barrier to obtain robust predictive models by high-throughput techniques (Vis-NIRS,
80 NIRS, MIRS, NMR) (de Oliveira et al., 2014; Fan et al., 2016; Pissard et al., 2012).
81 Particularly with the non-destructive and localized (around 2 cm²) NIR measurements
82 on apples, it is essential to know more about the distribution of components in fruit in
83 order to determine where and how many measurements are needed, as well as to
84 access the representative sample portion to be characterized using reference methods
85 for calibration dataset.

86 Hyperspectral imaging (HSI) is an emerging platform technique that integrates
87 imaging and spectroscopy to provide both spatial and spectral information (Gowen et
88 al., 2007). It is safer than X-ray imaging, more rapid and affordable than FT-IR
89 imaging and Magnetic resonance imaging, and with a better image quality than
90 thermal imaging (Fan et al., 2016; Ma et al., 2018). Until now, applications of HSI in
91 the Visible-NIR (400-1000 nm) or NIR (1000-2400 nm) ranges were carried out to
92 evaluate the variability of apple quality, such as fruit defects (Mehl et al., 2004),
93 firmness (Peng and Lu, 2008), mealiness (Huang and Lu, 2010) and soluble solids
94 content (Mendoza et al., 2011). These studies were applied nondestructively on apple
95 fruit. As the NIRS radiation penetration depth is around 0.2 to 0.3 cm in the spectral
96 area between 900 and 1900 nm (Lammertyn et al., 2000), the non-destructive

97 detection of HSI does not allow to evaluate the entire internal heterogeneity of apple
98 fruit. Thus, the HSI is used destructively by scanning fruit slices and makes possible
99 to describe the distribution of the internal soluble solids content, as shown in apples
100 (Mo et al., 2017) and melons (Sun et al., 2017). However, these studies need a large
101 number of reference data (numbers of samples and limited samples quantity) on all
102 the targeted areas of single fruit, required for model calibration.

103 Consequently, the main objective of this work was to provide a simple and
104 efficient method to reduce the intensive reference measurements (contents of dry
105 matter, total sugars, individual sugars, acids and polyphenols) in order to develop a
106 HSI modelling calibration and to evaluate the apple variability and heterogeneity.

107 **2. Material and methods**

108 2.1 Apple fruit

109 The experiment was conducted on four different apple varieties: ‘Golden
110 Delicious’ (GD), ‘Granny Smith’ (GS), ‘Braeburn’ (BR) and ‘Royal Gala’ (GA). In
111 2018, all apples were harvested in the experimental orchard at La Pugère (Bouches du
112 Rhône, France). ‘Braeburn’, ‘Granny Smith’ and ‘Royal Gala’ apples were grown
113 under a commercial fruit thinning (Th+, 50-100 fruit/ tree). ‘Golden Delicious’ apples
114 were grown under two thinning conditions, the commercial fruit thinning (Th+,
115 50-100 fruit/ tree) and without thinning (Th-, 150-200 fruit/ tree). After the
116 commercial harvesting (‘Royal Gala’ on August 28th, Golden Delicious on September
117 19th, ‘Granny Smith’ on September 20th, and ‘Braeburn’ on October 3rd), all apples
118 were stored in a cold chamber at 4 °C and at around 90 % of humidity until their

119 characterization (November 2018).

120 2.2 Samples preparation

121 A calibration dataset corresponded to the data of 30 apples with similar sizes (6
122 fruit \times 5 apple groups of GD Th-,GD Th+, GS, BR, GA) and scanned using the
123 NIR-HSI imaging system. Each apple was cut with a slicing tool along horizontal
124 direction to produce six apple slices, including five 1.2 cm thick slices (named slices
125 from 'A' to 'E' at the stem, equator and calyx directions) and the one residual piece of
126 varying thickness (named slice 'F' at the calyx positions). Hyperspectral images of
127 180 apple slices (5 apple groups \times 6 fruit \times 6 slices) were acquired and six cylindrical
128 1.6 cm diameter portions were extracted with a cookie cutter (numbered 1 to 6) from
129 each of the apple slices A to E, and five or six cylinders from the residual slice F (**Fig.**
130 **1**).

131 The cylinders were put immediately in liquid nitrogen prior to storage at -20 °C,
132 giving 35 to 36 cylinders per apple, following the previous works of Mo et al. (2017)
133 and Bureau et al. (2013). These cylinders were distributed with a systematic
134 repartition for each apple from the top to the bottom and from the sunny to the shady
135 faces. In total 1056 cylinders (5 apple groups \times 6 fruit \times 35-36 cylinders) were
136 numbered and stored (**Part 2.4.1**). After the extraction of all the cylinders, RGB
137 photos were taken on each apple slice in order to ensure the correct correspondence
138 between the cylinders and HSI images (**Fig. 1**).

139 2.3 Hyperspectral Imaging (HSI) System

140 A pushbroom (a line-scanning type) near infrared hyperspectral imaging system

141 (SPECIM, Oulu, Finland) was used to acquire the hyperspectral images of apple slices.
142 Particularly, this NIR-HSI system consisted of a SWIR camera (SWIR-CL-400-N25E,
143 SPECIM) covering the spectral range of 1000-2500 nm with a spectral resolution of
144 about 12 nm, an OLES 56 camera lens (SPECIM), an illumination source (halogen
145 lamps) and a translating scanner. All the image acquisition parameters (the exposure
146 time of camera, the scanning speed etc.) were controlled by the LUMO® software
147 from SPECIM. Before measurements, a reflectance calibration was performed by
148 recording a dark current image (0 % reflectance) with an internal shutter and a white
149 image using a reference standard close to 100 % reflectance (Spectralon® 100 %). To
150 reduce the impact of light and noise, the calibrated hyperspectral images could be
151 automatically obtained using the dark and white reference images, with the following
152 equation:

$$153 \quad R(\lambda) = \frac{R_0(\lambda) - R_d}{R_w - R_d} \times 100 \% \quad (1)$$

154 with R : the calibrated hyperspectral image data, R_0 : the raw image data, R_d and R_w :
155 the dark and white reference images, respectively.

156 All images were acquired in the reflectance mode and the final image size for
157 each kernel is $387 \times \text{xdim} \times 288$, the two first values representing pixel dimensions in
158 the x and y directions (field of view of 9.8×6.3 cm, with a spatial resolution of 225
159 μm) and the third value accounting for the number of spectral channels. The xdim
160 values varied according to the dimensions of apple slices. Each image was acquired in
161 about twenty seconds. As the beginning and ending wavelengths contained noise
162 caused by the instrument itself (Sun et al., 2017), the 258 bands from 990 to 2450 nm

163 were selected for further spectral analysis.

164 2.4 Imaging pre-processing

165 The pre-processing of the hyperspectral images and the selection of region of
166 interest (ROIs) were performed with Matlab 7.5 (Mathworks Inc. Natick, MA)
167 software using the SAISIR package (Cordella & Bertrand, 2014). Due to the high
168 volume of data, the processing of all images was not possible using a common
169 computer. In this way, 10,000 spectra were randomly extracted from the HSI images
170 of each apple slice, counting around one third of the total number of spectra in each
171 HSI image. Afterwards, all random selected spectra were gathered into a matrix X (5
172 apple groups \times 6 fruit \times 6 slices \times 10,000 rows by 258 columns). After pre-tests,
173 matrix X was smoothed by a window size of three pixels. A given value $x(i)$ of index i
174 was replaced by the local average of $x(i-1) + x(i) + x(i+1)$. Then it was
175 pre-processed with standard normal variate (SNV) to increase its signal to noise ratio
176 for the selection of ROIs.

177 2.5 ROI selection and characterization

178 PCA has been commonly applied on the NIR-HSI of agro-food products for
179 safety and quality assessments (Dale, et al., 2013). It was performed on the
180 pre-processed matrix X to check the major components causing variability in the
181 apples. Afterwards, this model was applied to all pixels of all images, and the major
182 components (PCs) were selected as estimators to refold into PCs images to point out
183 the heterogeneous areas in each HSI image of apple slice. Finally, the ROIs to be
184 analyzed by chemical and biochemical measurements (141 samples) were manually

185 selected depending on the results of the major principal components and the same
186 location on photographic images (an example of the ROIs marked black circles in
187 **Fig. 1**).

188 2.6 Chemical and biochemical measurements

189 All chemical and biochemical characterizations (contents of dry matter, fructose,
190 glucose, sucrose, malic acid and sum of polyphenols) were performed on these ROIs
191 (141 samples) and expressed as the ratio on fresh weight. Particularly, individual
192 sugars (glucose, fructose, and sucrose) and malic acid were quantified on the half of
193 each sample using an enzymatic method with commercial kits for food analysis,
194 following the manufacturer's instructions (R-biopharm, Darmstadt, Germany). The
195 total sugars content were computed by the sum of all individual sugars (fructose,
196 glucose and sucrose). The dry matter content (DMC) was estimated from the weight
197 of freeze-dried samples upon reaching a constant weight (freeze-drier, 3 days). The
198 freeze-dried samples were further used to quantify polyphenols by HPLC-DAD after
199 thioacidolysis as described in Le Bourvellec ([Le Bourvellec et al., 2011](#)). Particularly,
200 apple polyphenols were separated in an Agilent 1050 separation system coupled with
201 a (250 mm × 4 mm i.d.) Licrospher PR-18 5 µm column (Merck, Darmstadt,
202 Germany) operated at 30 °C. This data was presented as the sum of individual
203 polyphenols including procyanidins and monomeric flavanols, phenolic acids,
204 dihydrochalcones and flavonols.

205 2.7 Modelling

206 After smoothing with a 3-point window and the first order derivative with a 11

207 point window, the averaged spectra of each ROI (giving 141 spectra) and their related
208 reference data were used for modelling. Leave-one-out partial least squares
209 (LOO-PLS) regression was used to build prediction models with Matlab 7.5
210 (Mathworks Inc. Natick, MA) software using the SAISIR package (Cordella &
211 Bertrand, 2014). Random forest (RF) regression was also applied to compare the
212 prediction ability of developed models, using R software (version 4.0.2) (R Core
213 Team, 2019) coupled with several packages including ‘prospectr’ (Stevens and
214 Ramirez-Lopez, 2014), ‘Rmatlab’ (Bengtsson et al., 2018), ‘caret’ (Kuhn, 2015) and
215 ‘randomForest’ (Liaw and Wiener, 2002).

216 The developed model performance was assessed using the determination
217 coefficient of cross-validation (R_{cv}^2), the root mean square error of cross-validation
218 ($RMSE_{cv}$), the number of latent variables (LVs), the ratio of the standard deviation
219 values (RPD). The interpretations of beta-coefficients were used to determine the
220 relevant spectral regions. The spectral bands related to the maximum and minimum of
221 beta-coefficient values can present the most important wavelengths (Sun et al., 2017).

222 2.8 Prediction maps of apple quality attributes

223 After comparison of the modeling results of each apple quality attribute, only the
224 models with RPD values higher than 2.0 allowing a coarse quantitative prediction
225 (Nicolai et al., 2007), were selected to predict fruit quality attributes of all apple slices
226 at the individual pixel level. The prediction values were then visualized under the
227 form of prediction maps, which were used to phenotype the internal distributions of
228 the predicted quality attributes in apples.

229 **3 Results and discussion**

230 **3.1 Spectral characteristics**

231 The initial PCA conducted on the random selected spectra of one out of three
232 pixels of all apple slices (matrix X) was able to discriminate the variability and
233 heterogeneity of apple fruit between the top (slice A) and the bottom (slice F). The
234 first two principal components represented 68.0 % of the total variability, with the
235 first component (PC1) of 43.7 % and the second component (PC2) of 24.2 %,
236 respectively. For all apple groups, a clear discrimination was shown along the first
237 two principal components (PC1 and PC2) between the middle slices (slices C, D) and
238 the others (top slices A, B and bottom slices E, F). The most contributing wavelengths
239 of PC1 and PC2 were: i) the sharp peak around 1065 nm corresponding to the C-H
240 and O-H stretching in second overtone, which is linked to the sugar variations in fruit
241 (Sun et al., 2017); ii) the absorption region from 1157 - 1364 nm which is associated
242 with the first overtone of O-H band in water (Ignat et al., 2014); and iii) the broad
243 band at 1400-1530 nm which corresponds to the combination of second overtone of
244 C-H stretching and the first overtone of O-H stretching, already used to determine the
245 soluble solids content in apples (Zhang et al., 2019). These fingerprint wavelengths
246 pointed out the variations of water and carbohydrate contents in a single apple, which
247 were consistent with previous results using chemical measurements (Peiris et al., 1999;
248 Pissard et al., 2012).

249 In a second step, the variability expressed on the dominant PC1 components
250 (43.7 % of total variability) was used for phenotyping all apple slices based on a

251 correspondence between the different areas described by a color range, according to
252 their hyperspectral spectra. PC1 scores-images have directly pointed out the most
253 variable locations with the color range (**Fig. 1**). ROIs in each apple were targeted at
254 top slice A, middle slice C and bottom slice E, with the most different colored areas
255 (such as the area No. 3 of slice C and the area No. 3 of slice F in **Fig. 1**). Besides, the
256 clear color differences inside the middle slices (area No. 2 and No. 5 of slice D in **Fig.**
257 **1**) were also selected, depending on apple cultivars. A total of 141 ROIs was manually
258 selected and characterized by reference chemical measurements to check if these
259 targeted positions really showed variations consistent with the corresponding
260 hyperspectral images, and to identify the chemical components responsible for the
261 heterogeneity observed in PC1 scores images.

262 **3.2 Chemical characteristics of ROIs**

263 The boxplot of chemical reference data (**Fig. 2**) of the 141 selected ROIs showed
264 a large variation of contents of dry matter, total sugars, malic acid and polyphenols in
265 the different apple cultivars.

266 Royal Gala apples had the most intensive variations of DMC among the five
267 apple groups (**Fig. 2a**). Conversely, the lowest variations of DMC and of TSC (**Fig.**
268 **2b**) were observed in the thinned (GD Th+) and non-thinned Golden Delicious (GD
269 Th-), presenting a relatively limited heterogeneity of DMC and TSC in single GD
270 apples. The fructose content of Granny Smith (GS) had the lowest variations among
271 the four cultivars (**Fig. 2c**). Moreover, the contents of polyphenols varied a lot in each
272 apple cultivar (**Fig. 2f**). Golden Delicious (thinned and non-thinned) (0.34 ± 0.14 g/kg

273 in non-thinned GD and 0.34 ± 0.12 g/kg in thinned GD) and Royal Gala (GA) ($0.27 \pm$
274 0.14 g/kg) apples presented a large polyphenolic variation compared to GS apples
275 (0.55 ± 0.14 g/kg). This result was different from a previous work showing a small
276 internal heterogeneity of polyphenols in Gala (Vidot et al., 2019). This inconsistent
277 result could be due to the difference in the measured targeted areas in apples, only
278 parts close to the fruit surface (Vidot et al., 2019) versus parts distributed everywhere
279 inside the entire fruit (our experiment).

280 Concerning the effect of agricultural practices on Golden apple quality, the
281 average contents of total sugars and malic acid were higher in the thinning condition
282 (GD Th+) than in the non-thinning one (GD Th-), which was in line with our previous
283 results observed during the 2017 harvested season (Lan et al., 2020). Interestingly, the
284 tree thinning treatment, by increasing the individual apple growth potential, led to a
285 lower variability of malic acid (**Fig. 2f**) and sucrose (**Fig. 2d**) contents in Golden
286 Delicious apples, with the standard derivation values decreasing from 0.89 to 0.62
287 g/kg and from 10.9 to 9.3 g/kg, respectively.

288 Consequently, the most variable regions chosen according to the PC
289 scores-images truly exhibited a large heterogeneity, in agreement with the variations
290 of the reference values of total sugars, dry matter, malic acid and polyphenols. The
291 apple internal heterogeneity should be then considered as an important factor for
292 apple fruit quality characterization and understanding.

293 **3.3 Prediction of apple quality traits based on averaged spectra of ROIs**

294 The chemical composition data obtained on the 141 selected ROIs was used to

295 build prediction models validated within this selected subset, using the averaged
296 spectra of each ROI. Acceptable predictions of DMC (SD = 21.9 mg/g, $R_{cv}^2 = 0.83$,
297 $RMSE_{cv} = 9.7$ mg/g, RPD = 2.39) and TSC (SD = 18.7 g/kg, $R_{cv}^2 = 0.81$, $RMSE_{cv} =$
298 8.4 g/kg, RPD = 2.20) were obtained by LOO-PLS, respectively (**Table 1**). According
299 to Nicolai et al. (2007), a RPD over 2 indicates the possibility to a coarse qualitative
300 prediction of the internal attributes of fruit. The linear models (PLS) were much better
301 than the random forest (RF) (**Table1**), as described by Sun et al. (2017) to predict
302 soluble solids content in melon fruit. The small number of latent variables (LVs)
303 employed in PLS models indicated the robust prediction of DMC (LVs = 7) and TSC
304 (LVs = 5), based on data including different apple varieties and growing agricultural
305 practices. All predicted DMC and TSC on 141 ROIs by LOO-PLS regression were
306 well correlated to the measured values, according to their linearity correlation plots
307 (**Fig. 3a and 3b**). Moreover, the beta-coefficients showed strong positive or negative
308 bands (**Fig. 3c and 3d**) for both, the PLS regressions of DMC and TSC, including
309 informative spectral regions at around 1123 nm, 1208 nm, 1389- 1401 nm, 1474-
310 1480 nm, 1857- 1863 nm and 2319- 2336 nm, which have been widely reported to
311 estimate water and sugar contents in apple fruit (Giovannelli et al., 2014; Lan et al.,
312 2020; Peirs et al., 2003). Particularly, six sharp peaks at 1208 nm, 1123 nm, 1389 nm,
313 1474 nm, 1857 and 2336 nm were identified as being important wavelengths to
314 predict dry matter content in apples. And the specific wavelengths at 1123 nm, 1401
315 nm, 1480 nm, 1863 nm and 2319 nm contributed to the determination of total sugars
316 in apple tissues.

317 However, modelling using the averaged spectra of ROIs showed a limited ability
318 to predict the individual sugars (fructose, glucose and sucrose), malic acid and sum of
319 polyphenols (**Table 1**). This was expected and in agreement with the previous work
320 (Walsh et al., 2020). That could be due to i) their respective lower content in apple
321 tissues compared with DMC and TSC and ii) the limited chemical variations in our
322 studied apple varieties. Concerning polyphenols, a larger variation is observed in the
323 cider apple varieties from 1 to 7 g/kg in apple parenchyma (Sanoner et al., 1999) than
324 in the dessert varieties, such as those of this study, from 0.6 to 0.9 g/kg (Guyot et al.,
325 2002) because of their highest content in procyanidins, the main polyphenols. Thus, a
326 better prediction of these compounds might be obtained taking into account the entire
327 variability within apple varieties.

328 As mentioned in **section 3.1**, the fingerprint wavelengths of apple variability and
329 heterogeneity were mainly related to water and carbohydrates. Thus, for these five
330 apple groups (BR, GA, GS, thinned and non-thinned GD), prediction models based on
331 the averaged HSI spectra of ROIs and their reference values were suitable to estimate
332 intensive variations of water and the dominated soluble contents in apple fruit, such as
333 dry matter and total sugars, but not of individual compounds (fructose, glucose,
334 sucrose and malic acid) or microcomponents (sum of polyphenols).

335 **3.4 Phenotyping apple heterogeneity by HSI**

336 For a more in-depth assessment of the internal composition of each apple, the
337 best PLS models described in the **Part 3.2** were applied to predict the quality traits at
338 each pixel on all hyperspectral images of apple slices. The resulting images were

339 presented as ‘prediction maps’ for TSC (**Fig. 4**) for each apple slice. In total, 10 colors
340 were used to fit the different intervals of the predicted values and pixels with the
341 similar predicted values appeared in the same color. The prediction results
342 demonstrated a large variability and heterogeneity of total sugars and dry matter
343 contents i) in different apple varieties; ii) between individual apple fruit and iii) inside
344 single fruit.

345 For the traditional non-destructive NIR analyses on apples, to obtain a robust
346 prediction model, the calibration dataset should be sufficiently rich in variations,
347 particularly taking into account the existing variability with the fruit itself ([Zhang et](#)
348 [al., 2018](#)). Our prediction results provided advanced knowledge to determine where
349 and how many positions are needed with the non-destructively NIRS measurements
350 on apple surfaces, as well as to access the sample portion to be analyzed by reference
351 methods for the calibration set.

352 In the literature, NIR predictions of apple quality traits involve taking
353 measurements at up to four points located in the equatorial region ([Liu and Ying, 2005](#);
354 [Peirs et al., 2003](#); [Pissard et al., 2012](#)), or along the stem, equator and calyx positions
355 of apples ([Fan et al., 2016](#)). However, there was a reverse conclusion to reach the
356 accurate predictions of developed models following each of these two methods. From
357 our results, a specific attention needs to be paid according to the ‘cultivar’, which is
358 the major factor influencing the fruit heterogeneity and the possible reason to explain
359 the aforementioned disagreement result. According to the relative standard deviation
360 (RSD) values of the predicted DMC and TSC of all pixels in single apples, different

361 levels of internal chemical variations were observed in Braeburn (RSD of DMC =
362 24.6 % and of TSC = 22.1 %), Royal Gala (RSD of DMC = 26.5 % and of TSC =
363 27.1 %), Granny Smith (RSD of DMC = 18.9 % and of TSC = 22.0 %) and thinned
364 Golden Delicious (RSD of DMC = 13.2 % and of TSC = 15.7 %). These results
365 indicated the same and limited spectral measurement points for all apples could not
366 present such intensive internal quality variations of different cultivars. From a
367 spectroscopic point of view, an increase of measured positions on apple surfaces
368 therefore is particularly important to improve accuracy in the calibration steps.

369 In all apples, the large DMC and TSC differences among the middle (the average
370 predicted DMC of all pixels in slice C and D of all cultivars = 136.5 ± 16.2 g/kg and
371 TSC = 115.6 ± 14.3 g/kg), top (the average predicted DMC of all pixels in slice A and
372 B of all cultivars = 117.1 ± 22.4 g/kg and TSC = 79.5 ± 17.1 g/kg) and bottom slices
373 (the average predicted DMC of all pixels in slice E and F of all cultivars = $124.1 \pm$
374 25.2 g/kg and TSC = 87.3 ± 20.1 g/kg) demonstrated that four points at the equatorial
375 region might not be enough to provide the representative spectra of the entire apple
376 fruit. NIRS information from top to bottom of apple surfaces therefore needs to be
377 considered for all apple cultivars.

378 Consequently, the strong variability and heterogeneity of apples were highlighted
379 using our developed models, and probably constitute the major barrier to an accurate
380 NIR modelling. The similar distribution results of TSC and DMC in apple slices were
381 observed in most apple slices of each cultivar (at least 4 over 6 fruits). These results
382 provided an important opportunity to advance our knowledge on the quality

383 measurement: where and how many specific positions need to be measured on apple
384 surfaces with NIRS, in order to develop accurate and robust prediction models.

385 The previous HSI models mainly detected the soluble solids content and firmness
386 changes in single fruit (Mo et al., 2017; Sun et al., 2017), because of the quick and
387 easy reference data quantification of all targeted samples using digital refractometers
388 and hardness detectors. Compared to these studies, our work provided an efficient
389 solution for the HSI modelling calibration step, depending on the reference data
390 measured on 141 representative samples instead of the 1056 prepared samples.
391 Importantly, this method offered a new sight on contents of total sugars (sum of the
392 fructose, glucose and sucrose) and dry matter in apples, with a limited number of
393 complicated (individual sugars measured by spectrometry using enzymatic kits) and
394 time-consuming (at least 24 hours for freeze-drying) analyses for HSI modelling. In
395 future, such a rapid and efficient approach for HSI modelling calibration would be
396 helpful to detect the variations of apple internal quality parameters according to
397 different environmental conditions (crop load, irrigation, light penetration and
398 elevations of regions etc.—) and growing stages, and then contribute to an
399 improvement of apple quality and production. The objective at the end could be to
400 have a better knowledge of the apple homogeneity in order to manage them better for
401 fresh market and processing taking into account the sustainability of practices.

402 **4. Conclusion**

403 In this study, the power of chemometric methods was harnessed in a two-steps
404 procedure for mapping of apple fruit heterogeneity while minimizing the number of

405 chemical analyses. PCA of NIR-HSI data was used to scan the heterogeneity of apple
406 slices and to pin-point the best representing areas of the whole spectral variation. A
407 limited number of chemical measurements could then be carried out and exploited by
408 PLS regression to identify the underlying compositional information present in
409 NIR-HSI data at individual pixels. NIR-HSI coupled with PLS regression showed a
410 good ability to phenotype the distribution of dry matter content and total sugars
411 content in apple fruit. The prediction models developed with the reference values of
412 the most variable areas identified by PCA on HSI data were enough to assess the
413 variability and heterogeneity of apple global parameters, with acceptable precisions
414 (range of values). For dry matter and total sugars, the PLS results had a better ability
415 than the random forest ones to estimate their distributions in apple slices. With the
416 rapid scanning of apple slices and a limited number of chemical measurements, this
417 method showed the great advantages of a simple fruit sampling, less experimental
418 deviations caused by rapid oxidation of fruit, and a high efficiency of model
419 developments. This method opens the possibility to more systematically evaluate the
420 fruit variability and heterogeneity in future projects.

421 **Acknowledgements**

422 The authors thank Shouyang Liu, Xiuliang Jin, Jiantao Zhao, Patrice Reling,
423 Barbara Gouble, Line Touloumet, Marielle Boge, Caroline Garcia (INRAE, SQPOV
424 unit) for their technical help. The ‘Interfaces’ project is an Agropolis Fondation
425 Flashship project publicly funded through the ANR (French Research Agency) under
426 “Investissements d’Avenir” programme (ANR-10-LABX-01-001 Labex Agro,

427 coordinated by Agropolis Fondation). Weijie Lan was supported by a doctoral grant
428 from Chinese Scholarship Council.

429 **References**

- 430 Barritt, B.H., Rom, C.R., Konishi, B.J., Dilley, M.A., 1991. Light level influences spur quality and
431 canopy development and light interception influence fruit production in apple. *HortScience* 26,
432 993-999. <https://doi.org/10.21273/HORTSCI.26.8.993>.
- 433 Bengtsson, H., Jacobson, A., Riedy, J., Bengtsson, M.H., LazyLoad, T., ByteCompile, T., 2018.
434 Package 'R. matlab'.
- 435 Bureau, S., Ścibisz, I., Le Bourvellec, C., & Renard, C. M. G. C. (2012). Effect of Sample Preparation
436 on the Measurement of Sugars, Organic Acids, and Polyphenols in Apple Fruit by
437 Mid-infrared Spectroscopy. *J. Agric. Food Chem.* 60(14), 3551-3563.
438 <https://doi.org/10.1021/jf204785w>.
- 439 Cordella, C. B., & Bertrand, D. (2014). SAISIR: A new general chemometric toolbox. *TrAC Trends in*
440 *Analytical Chemistry*, 54, 75-82. <https://doi.org/10.1016/j.trac.2013.10.009>
- 441 Dale, L. M., Thewis, A., Boudry, C., Rotar, I., Dardenne, P., Baeten, V., & Pierna, J. A. F. (2013).
442 Hyperspectral Imaging Applications in Agriculture and Agro-Food Product Quality and Safety
443 Control: A Review. *Applied Spectroscopy Reviews*, 48(2), 142-159. <https://doi.org/10.1080/05704928.2012.705800>.
- 444
- 445 de Oliveira, G.A., Bureau, S., Renard, C.M.G.C, Pereira-Netto, A.B., de Castilhos, F., 2014.
446 Comparison of NIRS approach for prediction of internal quality traits in three fruit species.
447 *Food Chem.* 143, 223-230. <https://doi.org/10.1016/j.foodchem.2013.07.122>.
- 448 Fan, S., Zhang, B., Li, J., Huang, W., Wang, C., 2016. Effect of spectrum measurement position
449 variation on the robustness of NIR spectroscopy models for soluble solids content of apple.
450 *Biosystems Engineering* 143, 9-19. <https://doi.org/10.1016/j.biosystemseng.2015.12.012>.
- 451 Giovanelli, G., Sinelli, N., Beghi, R., Guidetti, R., Casiraghi, E., 2014. NIR spectroscopy for the
452 optimization of postharvest apple management. *Postharvest Biol. Technol.* 87, 13-20.
453 <https://doi.org/10.1016/j.postharvbio.2013.07.041>.
- 454 Gowen, A.A., O'Donnell, C.P., Cullen, P.J., Downey, G., Frias, J.M., 2007. Hyperspectral imaging – an
455 emerging process analytical tool for food quality and safety control. *Trends in Food Science &*
456 *Technology* 18, 590-598. <https://doi.org/10.1016/j.tifs.2007.06.001>.
- 457 Guyot, S., Le Bourvellec, C., Marnet, N., Drilleau, J., 2002. Procyanidins are the most abundant
458 polyphenols in dessert apples at maturity. *LWT-Food Science and Technology* 35, 289-291.
459 <https://doi.org/10.1006/fstl.2001.0843>.
- 460 Huang, M., Lu, R., 2010. Apple mealiness detection using hyperspectral scattering technique.
461 *Postharvest Biol. Technol.* 58, 168-175. <https://doi.org/10.1016/j.postharvbio.2010.08.002>.
- 462 Ignat, T., Lurie, S., Nyasordzi, J., Ostrovsky, V., Egozi, H., Hoffman, A., Friedman, H., Weksler, A.,
463 Schmilovitch, Z.e., 2014. Forecast of Apple Internal Quality Indices at Harvest and During
464 Storage by VIS-NIR Spectroscopy. *Food and Bioprocess Technology* 7, 2951-2961.
465 <https://doi.org/10.1007/s11947-014-1297-7>.
- 466 Kuhn, M., 2015. Caret: classification and regression training. *Astrophysics Source Code Library*.
- 467 Lammertyn, J., Peirs, A., De Baerdemaeker, J., Nicolai, B., 2000. Light penetration properties of NIR
468 radiation in fruit with respect to non-destructive quality assessment. *Postharvest Biol. Technol.*
469 18, 121-132. [https://doi.org/10.1016/S0925-5214\(99\)00071-X](https://doi.org/10.1016/S0925-5214(99)00071-X).
- 470 Lan, W., Jaillais, B., Leca, A., Renard, C.M.G.C., Bureau, S., 2020. A new application of NIR
471 spectroscopy to describe and predict purees quality from the non-destructive apple

472 measurements. *Food Chem.* 310, 125944. <https://doi.org/10.1016/j.foodchem.2019.125944>.

473 Le Bourvellec, C., Bouzerzour, K., Ginies, C., Regis, S., Plé, Y., Renard, C.M.G.C., 2011. Phenolic and
474 polysaccharidic composition of applesauce is close to that of apple flesh. *J Food Compost*
475 *Anal* 24, 537-547. <https://doi.org/10.1016/j.jfca.2010.12.012>.

476 Liaw, A., Wiener, M., 2002. Classification and regression by randomForest. *R news* 2, 18-22.

477 Liu, Y., Ying, Y., 2005. Use of FT-NIR spectrometry in non-invasive measurements of internal quality
478 of 'Fuji' apples. *Postharvest Biol. Technol.* 37, 65-71.
479 <http://doi.org/10.1016/j.postharvbio.2005.02.013>.

480 Ma, T., Li, X., Inagaki, T., Yang, H., Tsuchikawa, S., 2018. Noncontact evaluation of soluble solids
481 content in apples by near-infrared hyperspectral imaging. *J. Food Eng.* 224, 53-61.
482 <https://doi.org/10.1016/j.jfoodeng.2017.12.028>.

483 Mehl, P.M., Chen, Y.-R., Kim, M.S., Chan, D.E., 2004. Development of hyperspectral imaging
484 technique for the detection of apple surface defects and contaminations. *J. Food Eng.* 61,
485 67-81. [https://doi.org/10.1016/S0260-8774\(03\)00188-2](https://doi.org/10.1016/S0260-8774(03)00188-2).

486 Mendoza, F., Lu, R., Ariana, D., Cen, H., Bailey, B., 2011. Integrated spectral and image analysis of
487 hyperspectral scattering data for prediction of apple fruit firmness and soluble solids content.
488 *Postharvest Biol. Technol.* 62, 149-160. <https://doi.org/10.1016/j.postharvbio.2011.05.009>.

489 Menesatti, P., Zanella, A., D'Andrea, S., Costa, C., Paglia, G., Pallottino, F., 2009. Supervised
490 Multivariate Analysis of Hyper-spectral NIR Images to Evaluate the Starch Index of Apples.
491 *Food and Bioprocess Technology* 2, 308-314. <https://doi.org/10.1007/s11947-008-0120-8>.

492 Mo, C., Kim, M.S., Kim, G., Lim, J., Delwiche, S.R., Chao, K., Lee, H., Cho, B.-K., 2017. Spatial
493 assessment of soluble solid contents on apple slices using hyperspectral imaging. *Biosystems*
494 *engineering* 159, 10-21. <https://doi.org/10.1016/j.biosystemseng.2017.03.015>.

495 Nicolai, B.M., Beullens, K., Bobelyn, E., Peirs, A., Saeys, W., Theron, K.I., Lammertyn, J., 2007.
496 Nondestructive measurement of fruit and vegetable quality by means of NIR spectroscopy: A
497 review. *Postharvest Biol. Technol.* 46, 99-118. <https://doi.org/10.1016/j.postharvbio.2007.06.024>.

498

499 Peiris, K., Dull, G., Leffler, R., Kays, S., 1999. Spatial variability of soluble solids or dry-matter
500 content within individual fruits, bulbs, or tubers: implications for the development and use of
501 NIR spectrometric techniques. *HortScience* 34, 114-118. <https://doi.org/10.21273/HORTSCI.34.1.114>.

502

503 Peirs, A., Scheerlinck, N., Nicolai, B.M., 2003. Temperature compensation for near infrared reflectance
504 measurement of apple fruit soluble solids contents. *Postharvest Biol. Technol.* 30, 233-248.
505 [https://dx.doi.org/10.1016/S0925-5214\(03\)00118-2](https://dx.doi.org/10.1016/S0925-5214(03)00118-2).

506 Peng, J., Bi, J., Yi, J., Wu, X., Zhou, M., & Zhao, Y. (2019). Characteristics of cell wall pectic
507 polysaccharides affect textural properties of instant controlled pressure drop dried carrot chips
508 derived from different tissue zone. *Food chem.* 293, 358-367. <https://doi.org/10.1016/j.foodchem.2019.05.008>.

509

510 Peng, Y., Lu, R., 2008. Analysis of spatially resolved hyperspectral scattering images for assessing
511 apple fruit firmness and soluble solids content. *Postharvest Biol. Technol.* 48, 52-62.
512 <https://doi.org/10.1016/j.postharvbio.2007.09.019>.

513 Pissard, A., Baeten, V., Romnée, J.-M., Dupont, P., Mouteau, A., Lateur, M., 2012. Classical and NIR
514 measurements of the quality and nutritional parameters of apples: a methodological study of
515 intra-fruit variability. *BASE*. <https://popups.uliege.be:443/1780-4507/index.php?id=8782>.

516 R Core Team, R.C., 2019. R: A language and environment for statistical computing.
517 Sanoner, P., Guyot, S., Marnet, N., Molle, D., Drilleau, J.-F., 1999. Polyphenol profiles of French cider
518 apple varieties (*Malus domestica* sp.). *J. Agric. Food. Chem.* 47, 4847-4853. [https://doi.org/](https://doi.org/10.1021/jf990563y)
519 [10.1021/jf990563y](https://doi.org/10.1021/jf990563y).
520 Stevens, A., Ramirez-Lopez, L., 2014. An introduction to the prospectr package. R Package Vignette,
521 Report No.: R Package Version 0.1 3.
522 Sun, M., Zhang, D., Liu, L., Wang, Z., 2017. How to predict the sugariness and hardness of melons: A
523 near-infrared hyperspectral imaging method. *Food Chem.* 218, 413-421. [https://doi.org/](https://doi.org/10.1016/j.foodchem.2016.09.023)
524 [10.1016/j.foodchem.2016.09.023](https://doi.org/10.1016/j.foodchem.2016.09.023).
525 USDA, U., 2018. Fresh deciduous Fruit: World markets and trade (apples, grapes, & pears).
526 <https://usda.library.cornell.edu/concern/publications/1z40ks800?locale=en>
527 Vidot, K., Devaux, M.-F., Alvarado, C., Guyot, S., Jamme, F., Gaillard, C., Siret, R., Lahaye, M., 2019.
528 Phenolic distribution in apple epidermal and outer cortex tissue by multispectral deep-UV
529 autofluorescence cryo-imaging. *Plant Science* 283, 51-59. [https://doi.org/10.1016/j.plantsci.](https://doi.org/10.1016/j.plantsci.2019.02.003)
530 [2019.02.003](https://doi.org/10.1016/j.plantsci.2019.02.003).
531 Walsh, K.B., Blasco, J., Zude-Sasse, M., Sun, X., 2020. Visible-NIR 'point' spectroscopy in
532 postharvest fruit and vegetable assessment: The science behind three decades of commercial
533 use. *Postharvest Biol. Technol.* 168, 111246.
534 <https://doi.org/10.1016/j.postharvbio.2020.111246>.
535 Xia, Y., Fan, S., Li, J., Tian, X., Huang, W., Chen, L., 2020. Optimization and comparison of models
536 for prediction of soluble solids content in apple by online Vis/NIR transmission coupled with
537 diameter correction method. *Chemometrics and Intelligent Laboratory Systems* 201, 104017.
538 <https://doi.org/10.1016/j.chemolab.2020.104017>.
539 Zhang, B., Dai, D., Huang, J., Zhou, J., Gui, Q., Dai, F., 2018. Influence of physical and biological
540 variability and solution methods in fruit and vegetable quality nondestructive inspection by
541 using imaging and near-infrared spectroscopy techniques: A review. *Critical Reviews in Food*
542 *Science and Nutrition* 58, 2099-2118. <https://doi.org/10.1080/10408398.2017.1300789>.
543 Zhang, D., Xu, Y., Huang, W., Tian, X., Xia, Y., Xu, L., Fan, S., 2019. Nondestructive measurement of
544 soluble solids content in apple using near infrared hyperspectral imaging coupled with
545 wavelength selection algorithm. *Infrared Physics & Technology* 98, 297-304.
546 <https://doi.org/10.1016/j.infrared.2019.03.026>.
547

548 **Figure captions:**

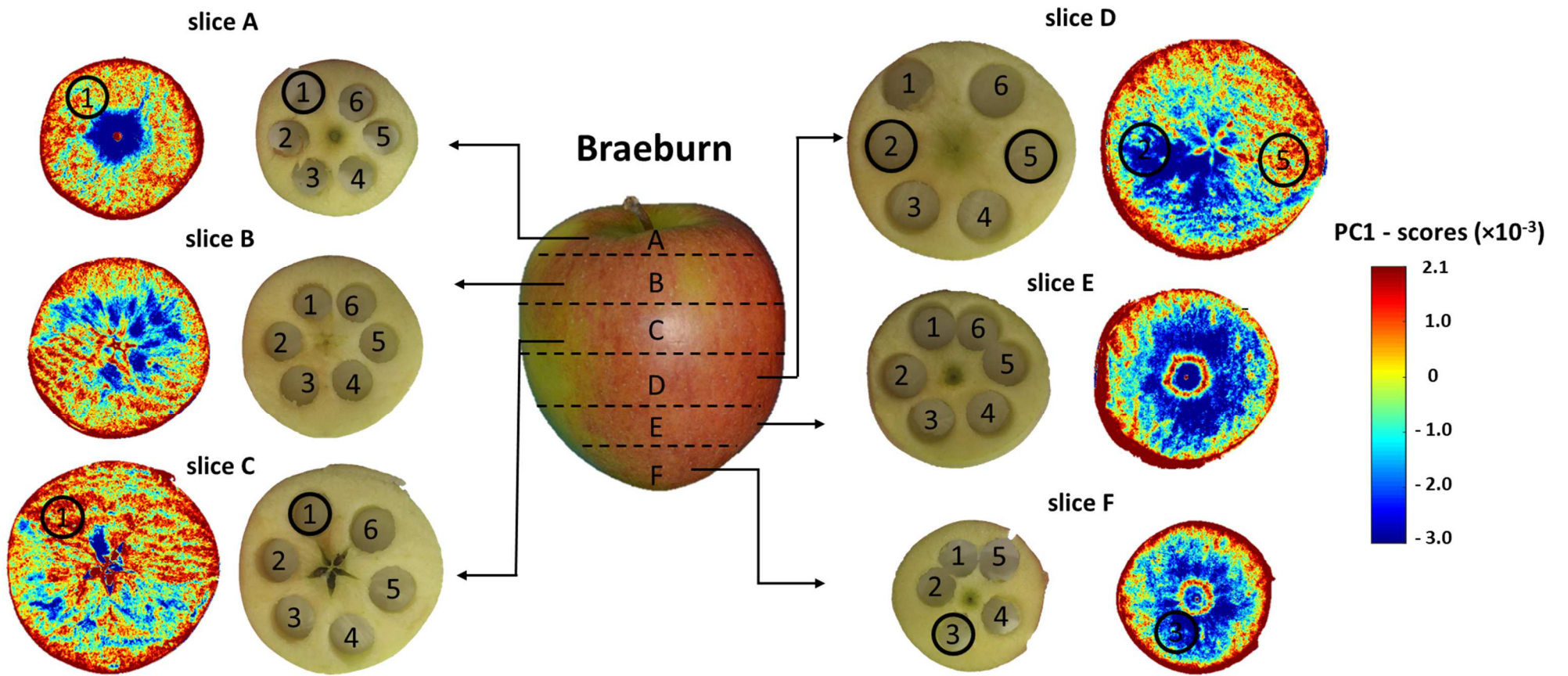
549 **Fig. 1.** The photographs of Braeburn apple slices and the first principal component
550 (PC1) score (from the PCA results on all apple groups) plot of all near-infrared
551 hyperspectral pixels (990- 2450 nm) for each slice (A, B, C, D, E, F). The selected
552 ROIs were labelled with black circles.

553 **Fig. 2.** The boxplots of: (a) dry matter, (b) total sugars, (c) fructose, (d) sucrose, (e)
554 glucose, (f) malic acid, (g) sum of polyphenols of ‘Braeburn’ (BR); ‘Granny Smith’
555 (G□); ‘Royal Gala’ (GA); thinned ‘Golden Delicious’ (GD Th+) and non-thinned
556 ‘Golden Delicious’ (GD Th-) apples.

557 **Fig. 3.** Comparison of the measured and the full-cross validated (a) dry matter content
558 (DMC) and (b) total sugars content (T□C) of the 141 ROI samples; and the most
559 contributing wavelengths for (c) DMC and (d) TSC prediction, using the
560 leave-one-out PLS regression on the ROI averaged spectra.

561 **Fig. 4.** The distribution of total sugars content (TSC) in apple slices predicted by the
562 LOO- PLS models developed based on the ROI averaged spectra.

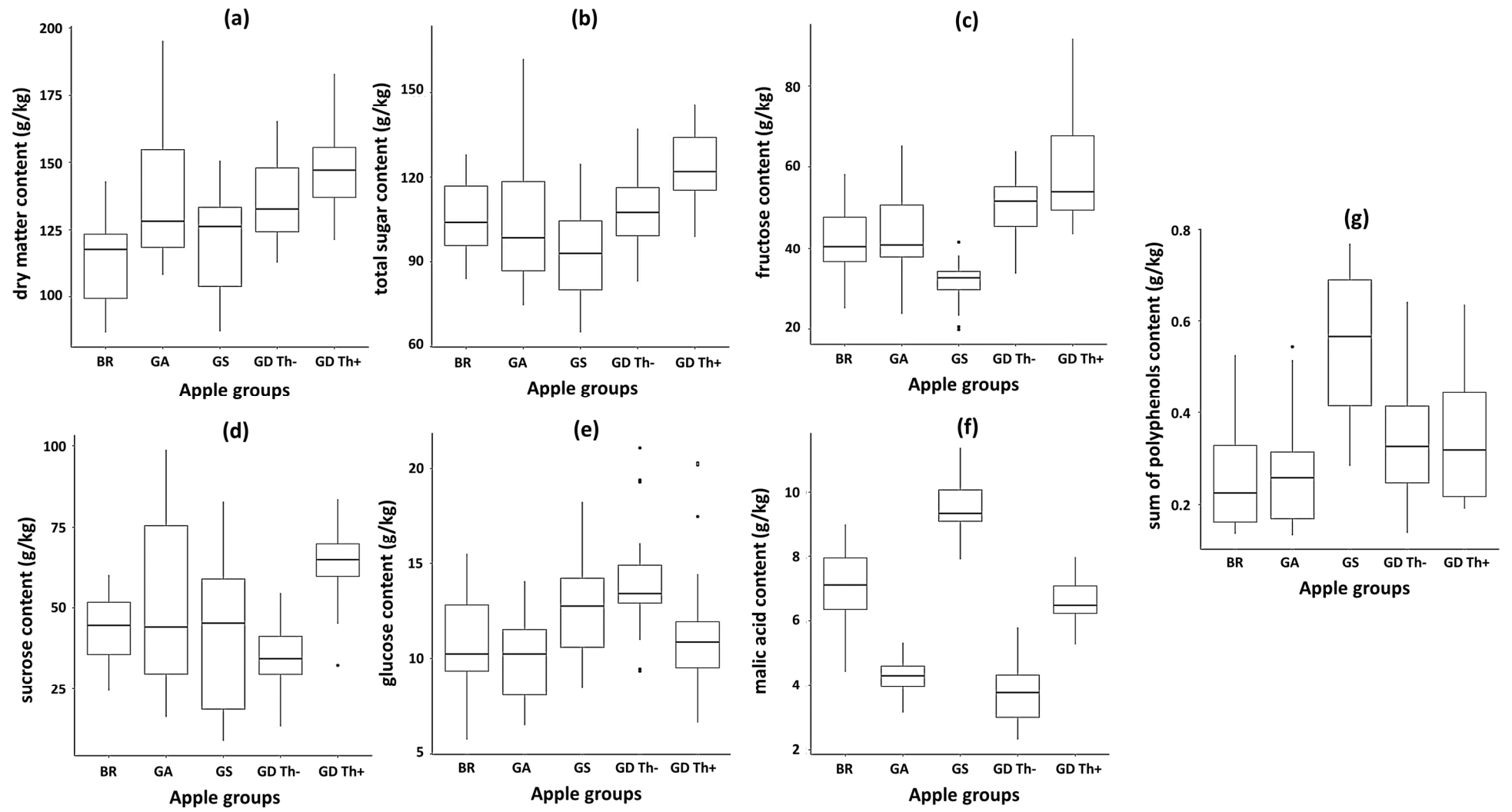
563



564

565

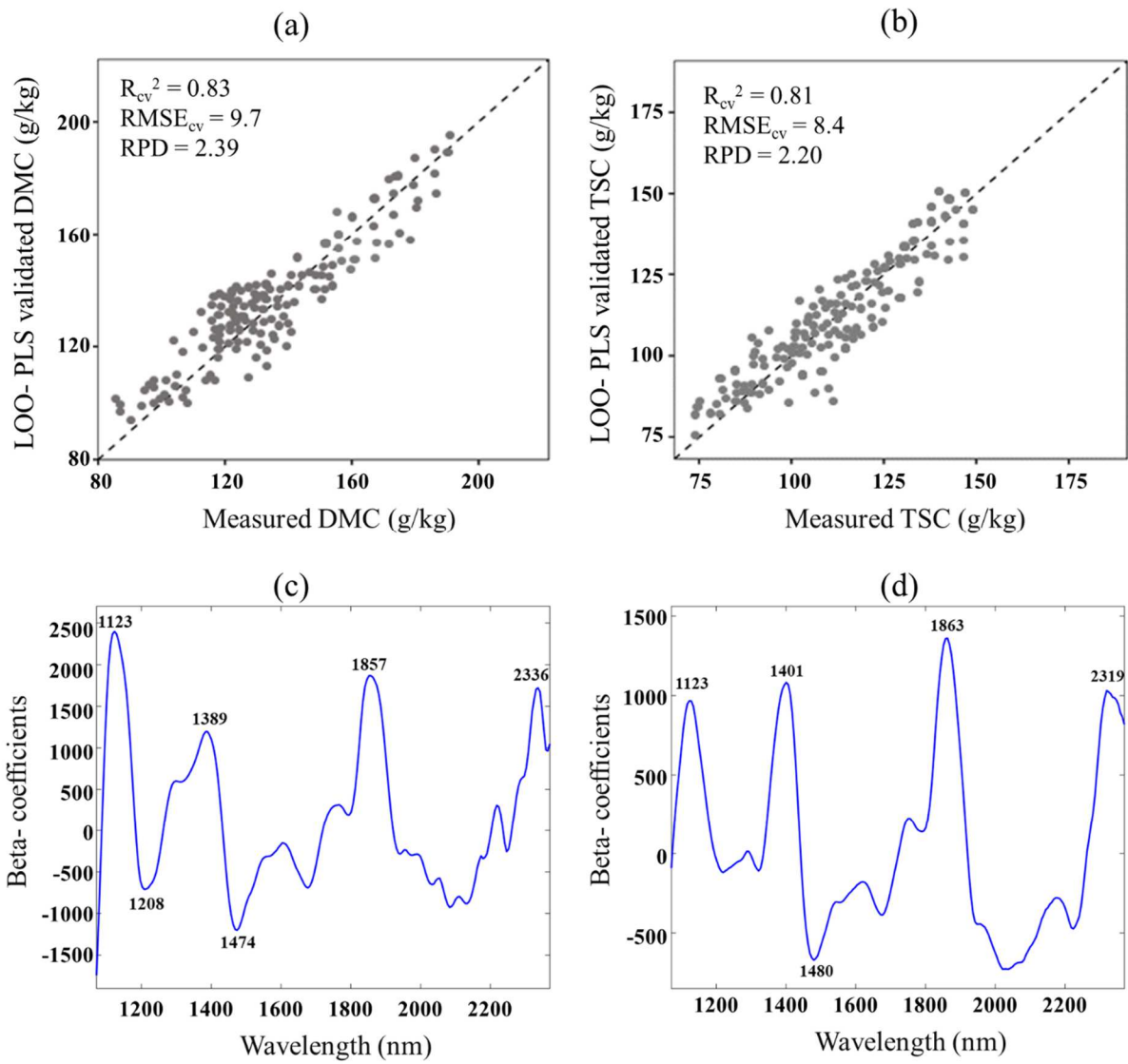
Fig. 1



566

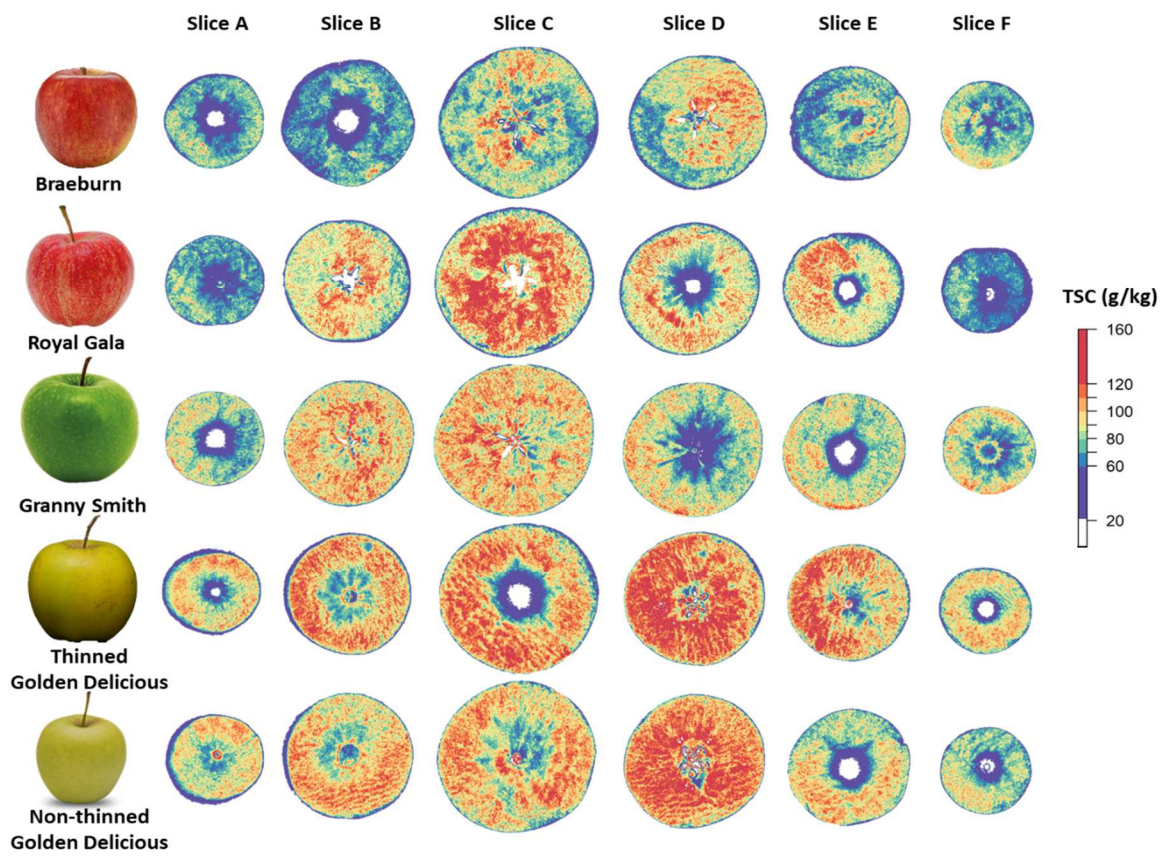
567

Fig. 2



568
569

Fig. 3



570

571

Fig. 4

572 **Table 1** Leave- one- out partial least square (LOO-PLS) and random forest (RF) results of apple internal quality traits using the averaged
 573 spectra of ROIs.

Parameters	Measured range	SD	Models	Full-crossed validation (n = 141)			
				R _{cv} ²	RMSE _{cv}	RPD	LVs
dry matter (mg/g)	86.2- 195.3	21.9	PLS	0.83	9.7	2.39	7
			RF	0.67	14.8	1.58	7
total sugars content (g/kg)	58.8- 156.8	18.7	PLS	0.81	8.4	2.20	5
			RF	0.78	9.2	2.11	4
fructose (g/kg)	19.8- 91.6	15.4	PLS	0.38	9.0	1.35	9
			RF	0.32	10.1	1.24	8
sucrose (g/kg)	9.1- 98.7	8.4	PLS	0.67	4.9	1.73	8
			RF	0.65	5.8	1.40	6
glucose (g/kg)	5.7- 21.1	3.0	PLS	0.29	2.5	1.19	6
			RF	0.27	2.5	1.18	6
malic acid (g/kg)	2.3- 11.4	2.2	PLS	0.31	2.1	1.23	7
			RF	0.15	2.3	1.08	8
Sum of polyphenols (g/kg)	0.13- 0.77	0.16	PLS	0.14	0.17	1.01	8
			RF	0.13	0.21	0.85	9

574

575

Graphical abstract

